

Wake structure of laminar flow past a sphere under the influence of a transverse magnetic field

Jun-Hua Pan¹, Nian-Mei Zhang¹ and Ming-Jiu Ni^{1,†}

¹School of Engineering Science, University of Chinese Academy of Sciences, Beijing 101408, PR China

(Received 5 June 2018; revised 21 May 2019; accepted 21 May 2019;
first published online 20 June 2019)

The wake structure of an incompressible, conducting, viscous fluid past an electrically insulating sphere affected by a transverse magnetic field is investigated numerically over flow regimes including steady and unsteady laminar flows at Reynolds numbers up to 300. For a steady axisymmetric flow affected by a transverse magnetic field, the wake structure is deemed to be a double plane symmetric state. For a periodic flow, unsteady vortex shedding is first suppressed and transitions to a steady plane symmetric state and then to a double plane symmetric pattern. Wake structures in the range $210 < Re \leq 300$ without a magnetic field have a symmetry plane. An angle θ exists between the orientation of this symmetry plane and the imposed transverse magnetic field. For a given transverse magnetic field, the final wake structure is found to be independent of the initial flow configuration with a different angle θ . However, the orientation of the symmetry plane tends to be perpendicular to the magnetic field, which implies that the transverse magnetic field can control the orientation of the wake structure of a free-moving sphere and change the direction of its horizontal motion by a field–wake–trajectory control mechanism. An interesting ‘reversion phenomenon’ is found, where the wake structure of the sphere at a higher Reynolds number and a certain magnetic interaction parameter (N) corresponds to a lower Reynolds number with a lower N value. Furthermore, the drag coefficient is proportional to $N^{2/3}$ for weak magnetic fields or to $N^{1/2}$ for strong magnetic fields, where the threshold value between these two regimes is approximately $N = 4$.

Key words: magnetohydrodynamics, particle/fluid flows

1. Introduction

The Lorentz force as a non-contact control method has received special attention in metallurgy. One application is to produce clean metal, excluding oxides and other types of non-metallic particles (El-Kaddah, Patel & Natarajan 1995). Another is to produce immiscible alloys with uniform distributions of solid particles in the matrix (Zheng *et al.* 2015). Such processes can be modelled as the transport of spherical non-conductive particles in magnetohydrodynamic (MHD) flow. It is noted that this is a first approximation, as more work needs to be done in the future on the transport of

† Email address for correspondence: mjni@ucas.ac.cn

anisotropic or electrically conducting particles. The wake structure behind the sphere is important since its trajectory is closely related to the wake structure (Ern *et al.* 2012). The wake of a flow past a fixed sphere will provide useful insight into the vortex dynamics of a free-moving body since, in the case of a moving sphere, one can assume to be standing at the sphere centre to observe the flow field. For example, when $Re < 210$, the wake of a flow past a fixed sphere is axisymmetric (Johnson & Patel 1999), which is unable to exert any side force on the sphere. Hence, a free-moving sphere with identical Reynolds number will rise vertically (see figure 27 in Horowitz & Williamson (2010)). The regime of an oblique trajectory (see figure 27 in Horowitz & Williamson (2010)) occurs in the range $210 < Re < 260$, in which the wake in the fixed-sphere case shows plane symmetry with counter-rotating vortices (Johnson & Patel 1999). The recirculation region behind the sphere is tilted, producing a constant lift force within the symmetry plane. If the sphere is unrestrained, the constant lift force will result in an oblique trajectory. Therefore, investigating the influence of a magnetic field on the wake structure behind a stationary sphere is the first step to understanding the vortex dynamics of a free sphere transported in MHD flows.

Any movement of a conducting fluid that is non-parallel to an external magnetic field will generate electric currents. Consequently, these currents will interact with the magnetic field to create the Lorentz force (Davidson 2001), which can greatly modify the flow pattern. Previous investigations have been reported for MHD flows with an obstacle, such as a grid bar (Branover, Eidelman & Nagorny 1995), a square cylinder (Mück *et al.* 2000) and cylinders with various orientations of magnetic fields, e.g. streamwise direction (Lahjomri, Capéran & Alemany 1993), transverse direction (Mutschke *et al.* 2001) and direction along the cylinder axis (Frank, Barleon & Müller 2001; Kanaris *et al.* 2013). As for the case of a sphere, Chester (1957) studied the effect of a magnetic field on the drag coefficient in a Stokes flow. An Oseen approximation method was extended to a perfectly conducting, viscous MHD flow in Goldsworthy (1961). Yonas (1967) made direct drag measurements on a sphere in conducting liquid sodium with a streamwise magnetic field and found that the drag coefficient was proportional to the interaction parameter $N^{1/2}$ for a strong magnetic field. They also observed that a relatively weak magnetic field was able to completely damp the dominant frequencies that had existed in hydrodynamic situations. This meant that the Lorentz force did suppress the unsteady flow. Similar phenomena were reported in Maxworthy (1962). Sekhar, Sivakumar & Kumar (2005) reported a two-dimensional axisymmetric model for steady and axisymmetric situations.

However, investigations related to clear wake structures behind a sphere affected by a magnetic field are rather scarce. Intuitive optical flow visualization techniques, such as dye visualization or particle image velocimetry (PIV) technology, cannot be applied due to the opacity of the liquid metal. Therefore, numerical simulation seems to be a useful method. Previous results (Pan, Zhang & Ni 2018) found five wake structure patterns and their transitions behind a sphere at Reynolds numbers up to 300 under the influence of a streamwise magnetic field. It was shown that the magnetic field had a great influence on the wake structure behind the sphere. Furthermore, for the cylinder cases, the orientation of the magnetic field had a dramatic influence on the wake structure. Therefore, we investigate the influence of a transverse magnetic field on wake structures behind a sphere.

Investigations of wake structures and instabilities of a flow past a fixed sphere without a magnetic field have been carried out, such as stability analyses (Natarajan & Acrivos 1993; Pier 2008), direct numerical simulations (Johnson & Patel 1999;

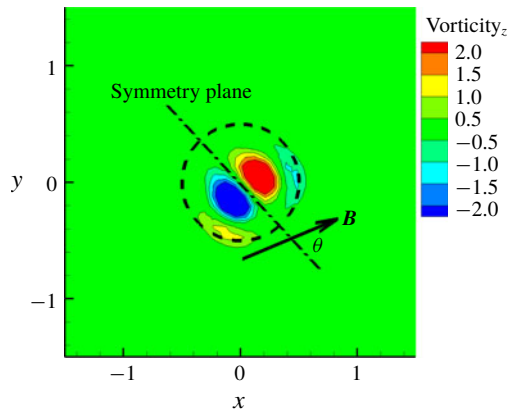


FIGURE 1. Cross-sectional plot of streamwise vortical structures at 1.5 diameters behind a sphere at $Re = 300$. The sphere profile is indicated by a dashed circle. There is an angle θ between the symmetry plane (dash-dotted line) and the transverse magnetic field B (arrow).

Re	Nature of flow	State
$20 \leq Re < 210$	Closed attached recirculation	Steady, axisymmetric
$Re \approx 210$	Axisymmetric \rightarrow plane symmetric	First bifurcation
$210 < Re < 270$	Stable double threads	Steady, plane symmetric
$Re \approx 270$	Steady \rightarrow unsteady	Second bifurcation
$270 < Re \leq 300$	Periodic vortex shedding	Unsteady, plane symmetric

TABLE 1. Summary of transitions with Reynolds numbers up to 300.

Tomboulides & Orszag 2000) and detailed experiments (Ormières & Provansal 1999). They all found a consistent scenario of transition. The wake structure transitions from axisymmetric to plane symmetric with double threads at $Re \approx 210$. This double-thread wake consists of a pair of steady streamwise counter-rotating vortices. The recirculation region behind the sphere is tilted and the shifting of this ring vortex makes the flow become non-axisymmetric. Subsequently, a second transition occurs at $Re \approx 270$. The double-thread wake is itself observed to become unstable in a periodic state within a symmetry plane determined by the first transition. It is called reflectional symmetry preserving (Fabre, Auguste & Magnaudet 2008). With increasing Reynolds number, hairpin vortices begin to shed from the sphere, e.g. dye lines in experiment (Johnson & Patel 1999) revealed shedding of large-amplitude hairpin vortices at $Re = 300$. As the Reynolds number is further increased, simulation in Mittal (1999) shows that the wake becomes irregular and no plane symmetry remains for $Re > 355$.

As reviewed above, with Reynolds numbers up to 300, the wake structure behind a sphere without a magnetic field will undergo a series of well-defined transitions, as given in table 1. The current work is to investigate how a transverse magnetic field affects the fluid dynamics and wake structures of these flows. Wake structures behind the sphere are plane symmetric at $210 < Re \leq 300$ in the absence of a magnetic field. Figure 1 plots a cross-section of streamwise vortical structures at 1.5 diameters behind the sphere at $Re = 300$. A symmetry plane is clearly shown. Its orientation is,

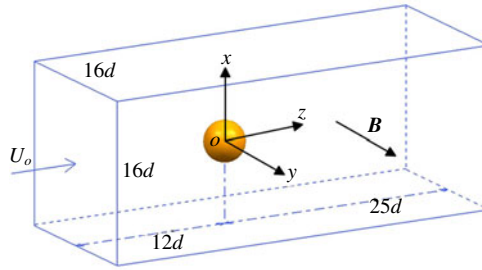


FIGURE 2. Schematic for the flow configuration and related geometrical parameters.

in principle, random but is determined by perturbations in experiment or numerical bias (Johnson & Patel 1999). After imposing a transverse magnetic field, there will be an angle between the symmetry plane and the transverse magnetic field; see angle θ in figure 1. Of particular interest in this work is to investigate whether the initial angle θ will affect the wake structure.

2. Flow configuration and modelling

An electrically conducting incompressible Newtonian fluid is considered under the influence of an imposed transverse magnetic field. For most cases of liquid-metal flow in industrial applications, the magnetic Reynolds number, which characterizes the ratio between magnetic convection and diffusion, is very small, $Rm = \mu\sigma UL \ll 1$. A so-called quasi-static approximation (Davidson 2001; Sarris *et al.* 2006; Moreau 2013) of MHD equations is invoked. The non-dimensional MHD equations governing the flow can be written as

$$\frac{\partial \mathbf{u}}{\partial t} + (\mathbf{u} \cdot \nabla) \mathbf{u} = -\nabla p + \frac{1}{Re} \nabla^2 \mathbf{u} + N(\mathbf{J} \times \mathbf{B}), \quad (2.1)$$

$$\nabla \cdot \mathbf{u} = 0, \quad (2.2)$$

$$\mathbf{J} = -\nabla \phi + \mathbf{u} \times \mathbf{B}, \quad (2.3)$$

$$\nabla \cdot \mathbf{J} = 0. \quad (2.4)$$

With the solenoidal current field (2.4) and the Ohm's law (2.3), a Poisson equation for the electric potential can be derived as

$$\nabla \cdot \nabla \phi = \nabla \cdot (\mathbf{u} \times \mathbf{B}). \quad (2.5)$$

The dimensionless flow variables, such as time t , velocity \mathbf{u} , pressure p , current density \mathbf{J} , imposed magnetic field \mathbf{B} and electric potential ϕ , are scaled with d/U_0 , U_0 , ρU_0^2 , $\sigma U B_0$, B_0 and $dU_0 B$, respectively. Here d , U_0 , ρ , σ , ν , μ and B_0 are the sphere diameter, uniform inflow velocity, fluid density, electrical conductivity, kinematic viscosity, magnetic permeability and the intensity of the magnetic field, respectively. Two dimensionless parameters in the momentum equation (2.1) are the Reynolds number $Re = U_0 d / \nu$ and the interaction parameter $N = \sigma d B^2 / \rho U_0$, which measure the ratios of inertial to viscous forces and electromagnetic to inertial forces, respectively.

Figure 2 shows the flow configuration and related geometrical parameters. A uniform inflow is along the z -axis, while a transverse magnetic field is in the x - y

plane. A concentric sphere-type grid is first clustered around the sphere to have good orthogonality. Then ‘O’ grids and multi-block grids are divided into other parts of the computational domain. A second-order-accurate consistent and conservative numerical scheme is sufficient to solve the present problem, in which the current density flux is located on the cell face while all other variables are stored in the cell centre. Detailed validation and verification can be found in Ni *et al.* (2007). Since the present work mainly investigates the influence of a transverse magnetic field on the wake structure at the rear of a sphere, any wake–wall interactions are not considered. Hence, slip boundary conditions are set on the lateral boundaries. A uniform velocity is given at the inlet, while a convective boundary condition is applied at the outlet. A no-slip boundary condition is imposed on the sphere. Furthermore, electric potential boundaries should be specified for the electric potential governing equation. All electric potential boundary conditions can be summarized as

$$\frac{\partial \phi}{\partial n} = (\mathbf{u} \times \mathbf{B}) \cdot \mathbf{n}, \quad (2.6)$$

which is derived from the electric potential (2.5) projected on the boundary. Here \mathbf{n} is the outward normal direction. The above equation derives the zero normal component of the current at the boundary, which implies that the lateral walls are insulators. It is suitable for practical situations since the duct flow with insulating walls is easily driven with less pressure drop (Müller & Bühler 2013). It is noted that currents will concentrate near the sphere and the present computational domain is sufficient to solve the physical mechanism. For the present fixed electrically insulating sphere, the boundary condition (2.6) on the sphere can be reduced to $\partial \phi / \partial n = 0$. The grid resolution test for the streamwise magnetic field case in Pan *et al.* (2018) can be re-used here.

The flow without a magnetic field is first simulated for a long time until a ‘stable’ state is obtained. Then, a uniform transverse magnetic field is imposed. The flow configuration and the numerical model are axisymmetric, and the axisymmetric flow in the absence of a magnetic field can be broken by different bifurcation points with increasing Reynolds number. When a transverse magnetic field is applied, we can expect symmetries with respect to two planes, which are parallel to the z -axis, and either parallel or normal to the magnetic field. One symmetry plane that is parallel to the magnetic field is named the P-symmetry plane and the other that is normal to the magnetic field is named the N-symmetry plane. The present discussion concerns Reynolds numbers up to 300, for which the wake structure behind the sphere will be steady axisymmetric, steady plane symmetric and periodic. The last two wake patterns have a symmetry plane whose orientation is, in principle, random, but is determined by certain numerical biases. As shown in figure 1, an angle θ exists after imposing a transverse magnetic field in the x – y plane. For a certain orientation of the symmetry plane, in order to check the dependence of the initial flow configuration with a different angle θ , x -directional and y -directional transverse magnetic fields with identical intensity are imposed respectively to investigate whether they have the same influences on the wake structure.

3. Results and discussions

3.1. Steady axisymmetric flow with magnetic field

When $20 < Re < 210$ in the absence of a magnetic field, the flow is steady, axisymmetric and topologically similar. Only the separation length and the separation

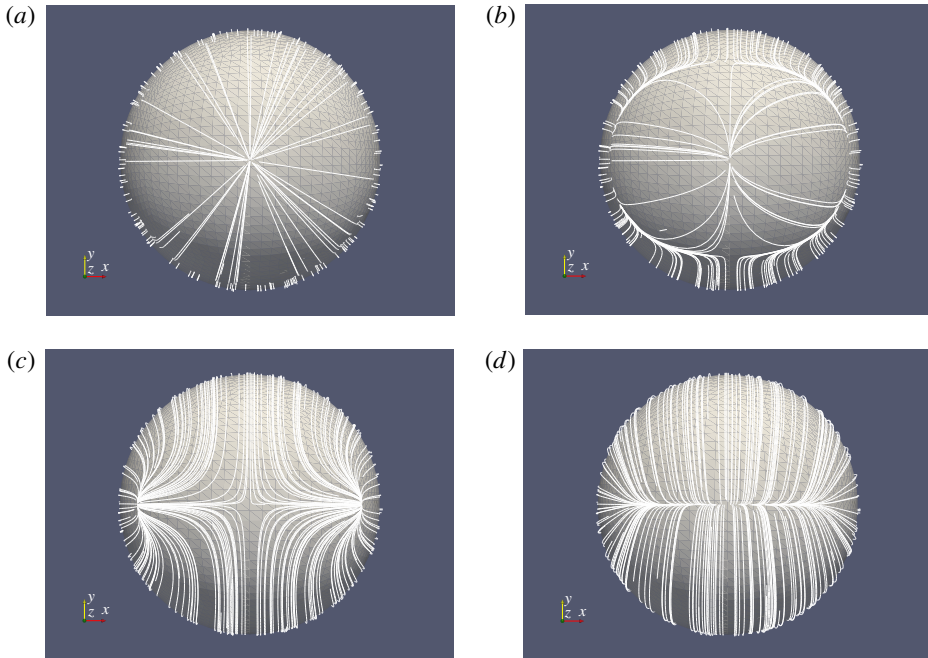


FIGURE 3. Skin friction lines on the sphere surface at $Re = 150$ with different interaction parameters: (a) $N = 0$, (b) $N = 0.3$, (c) $N = 1$ and (d) $N = 4$. The flow direction is from inside to outside. The magnetic field direction is from bottom to top.

angle of the separation bubble vary with different Reynolds numbers. Here, only the case at $Re = 150$ is considered. Since the flow is axisymmetric, any magnetic field direction in the transverse plane has the same effect on the wake structure. So only results of the y -directional transverse magnetic field are given below. Skin friction lines on the sphere surface with different interaction parameters are presented in figure 3. It is noted that convergence of skin friction lines is a criterion of three-dimensional flow separation (Lighthill 1963). Skin friction lines can clearly show flow traces in the rear of the sphere, which help us analyse the wake structure. As shown in figure 3, the shape of the flow separation line is narrowed in the P-symmetry plane at $N = 0.3$, which changes from a circular shape at $N = 0$ to an approximately elliptical shape. At this stage, the flow separation line is closed; skin friction lines in the inner part of the closed separation line come from recirculation flows. This means that a recirculation region still exists. However, with an increasing magnetic field at $N = 1$, the closed separation line disappears, which means the recirculation region is gone. Shatrov, Mutschke & Gerbeth (1997) also found that a transverse magnetic field could lead to a complete suppression of recirculation on a two-dimensional flow past a cylinder. Now the upstream flow converges into two symmetric points at the rear of the sphere surface. Further increasing the magnetic field at $N = 4$, the convergence points disappear and a straight separation line in the N-symmetry plane is clearly visible. Obviously, the non-axisymmetry of the wake structure is expected when affected by a transverse magnetic field. Now the wake structure is double plane symmetric and its symmetry planes are P- and N-symmetry planes.

Assuming that the sphere is absent in the flow, currents coming from electromotive forces are dominant in the core flow, which are generated by the fluid motion and

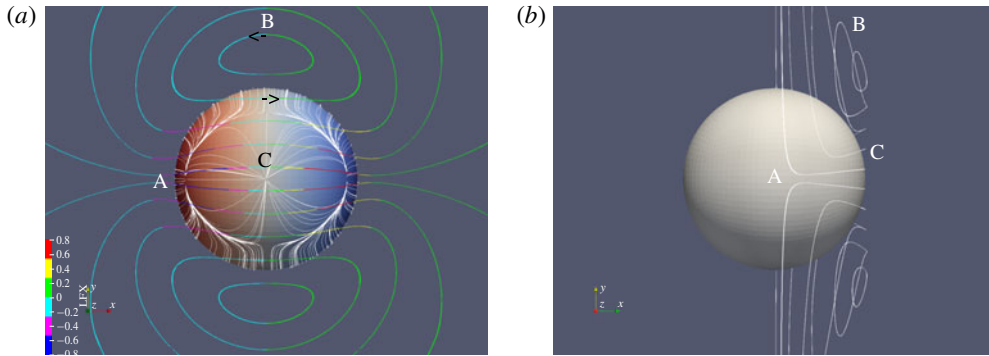


FIGURE 4. Current lines at $Re = 150$ with $N = 1$. The results are plotted at time instant $T_i = 7\Delta t$ after imposing a transverse magnetic field. Here Δt is the time step in the simulation. The magnetic field direction is from bottom to top. (a) Front view. The flow direction is from inside to outside. Current lines are contoured with x component of the Lorentz force, for which the positive direction is from left to right. The sphere is contoured with the electric potential, for which the red colour means positive value while the blue one represents negative value. (b) Side view. The flow direction is from left to right.

represented by $\mathbf{u} \times \mathbf{B}$ in the Ohm's law (2.3). When considering a sphere, the flow field mainly can be divided into two parts. One part is far away from the sphere, where electromotive forces $\mathbf{u} \times \mathbf{B}$ are dominant. Currents in this part flow from right to left, as shown at the B position of figure 4(a). The other part is near the sphere, where the velocity \mathbf{u} must be weaker. Positive charges are concentrated in the left side of the sphere (red colour) while negative charges are concentrated in the right side of the sphere (blue colour). The charge conservation law requires that current lines need to be closed. Since velocity is weaker here, electric potential gradients are dominant, where currents flow from left to right, as shown at the C position of figure 4(a). Furthermore, the sphere is electrically insulating. Currents will not go into the sphere, but flow over the surface instead, as shown from A to C positions in the side view of figure 4(b).

After understanding the current distribution, it is easy to know the Lorentz force $\mathbf{J} \times \mathbf{B}$ exerted on the flow. Since currents flow over the sphere surface from A to C positions in figure 4(b), the z -component of current J_z exists and will interact with the magnetic field to generate the x -component of the Lorentz force. Figure 4(a) shows the x -component of the Lorentz force contours on the current lines. These forces pull the upstream flow away from the P-symmetry plane to two lateral sides of the sphere. Figure 5(a) shows a schematic for the x -component of the Lorentz force acting on the upstream flow at a small interaction parameter. As a result, the upstream flow around the sphere diverges from the P-symmetry plane and converges to the N-symmetry plane. The blue curved arrows in figure 5(a) show this moving trend. The Lorentz force at position C of figure 4(a) is interesting – it will accelerate rather than damp the upstream flow. The z -component of the Lorentz force contours are plotted in figure 5(b). The z -component of the Lorentz force in zone D is larger than that in zone E since the currents are clustered in zone D, which corresponds to a faster flow near the surface in zone D. Hence this flow drives the flow separation line from a circular shape into an approximately elliptical shape, as shown in figure 4(a).

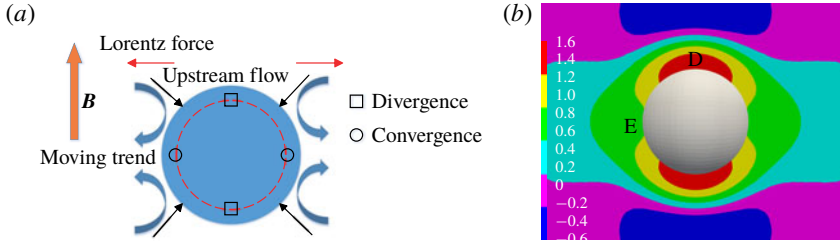


FIGURE 5. Lorentz force at $Re = 150$ with $N = 1$ in a front view for figure 4(a). The flow direction is from inside to outside. (a) Schematic for the Lorentz force acting on the upstream flow with a small interaction parameter. The red dashed line represents the separation line. The black and red arrows represent the upstream flow projected on the transverse plane and the Lorentz force on the transverse plane, respectively. The blue curved arrow shows the moving trend of the upstream flow affected by the Lorentz force. (b) The z -component of the Lorentz force contours in a section $0.35d$ away from the sphere centre.

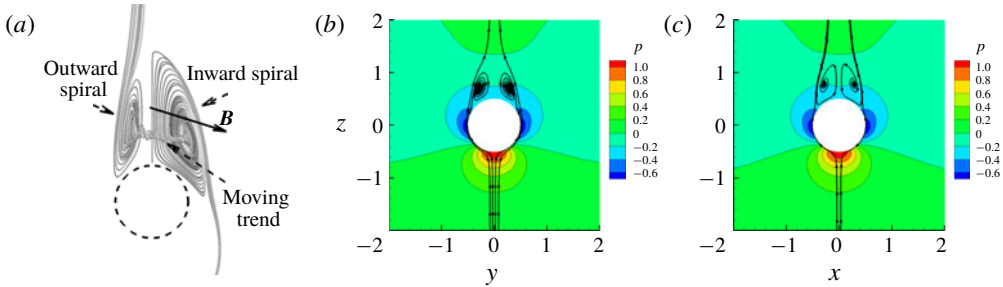


FIGURE 6. Pressure contours and streamlines in the symmetry plane at $Re = 150$ with $N = 0.1$. The magnetic field direction is along the y -axis. (a) One quarter of the three-dimensional streamlines. (b) P-symmetry plane. (c) N-symmetry plane.

Figure 6 shows such a recirculation of elliptical shape in detail. One quarter of the three-dimensional streamlines at $N = 0.1$ behind the sphere are plotted in figure 6(a). The direction of the core flow connecting two spirals reflects the moving trend of the upstream flow around the sphere. Such a moving trend will squeeze flow in the N-symmetry plane and make the left vortex in figure 6(a) spiral outwards. At the same time, the right vortex spirals inwards as it serves as the source of the core flow. Figures 6(b) and 6(c) show such spirals in the P- and N-symmetry plane. These two spirals will become smaller and finally disappear with increasing magnetic field.

Continuing with figure 4(a), figure 7 shows the time evolution of skin friction lines on the sphere surface. The recirculation region first becomes smaller in figure 7(a) and then disappears in figure 7(b). Now the upstream flow directly flows over the sphere surface and converges at the N-symmetry plane. At this stage, the x -component Lorentz force competes with the pressure gradient between the front and rear of the sphere, for which the Lorentz force pulls away the upstream flow from the P-symmetry plane and the pressure gradient pushes the upstream flow towards the P-symmetry plane. When the x -component Lorentz force is dominant, upstream flows will go away from the P-symmetry plane and converge at two points, as shown in figure 7(c). Further increasing the magnetic field, pressure gradients become dominant

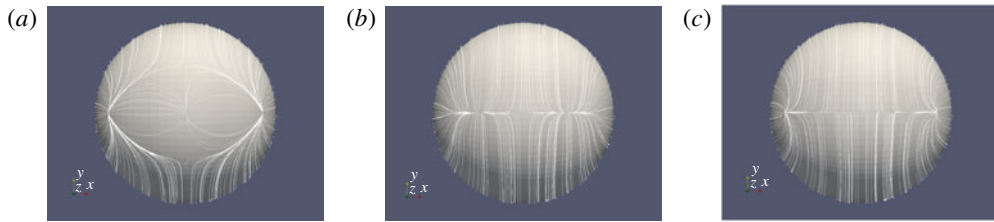


FIGURE 7. Time evolution of skin friction lines on the sphere surface at $Re = 150$ with $N = 1$. The results are plotted at different time instants after imposing a transverse magnetic field: (a) $T_i = 27\Delta t$, (b) $T_i = 167\Delta t$ and (c) $T_i = 267\Delta t$, where Δt is the time step in the simulation. The flow direction is from inside to outside. The magnetic field direction is from bottom to top.

and a straight separation line will remain at the N-symmetry plane. The final stable states in figures 3(c) and 3(d) correspond to these two situations.

3.2. Unsteady plane symmetric flow with magnetic field

3.2.1. Unsteady flow with weak magnetic field

It is known that the onset of unsteadiness for a flow past a sphere without a magnetic field occurs at $Re \approx 270$ and large-scale vortical structures are shed periodically at $Re = 300$. Regardless of the certain orientation of the symmetry plane, x -directional and y -directional transverse magnetic fields are imposed, respectively. For a weak magnetic field situation, the flow is still unsteady with vortex shedding. In order to quantify how the Lorentz force damps vortex shedding, a distance length H defined in Pan *et al.* (2018) is used here, which presents the tilt of recirculation behind the sphere, as shown in figure 8(a). In a period of vortex shedding, the tilt of recirculation varies with time. Time evolution of the distance length for different interaction parameters during one period is plotted in figure 8(b). The amplitude is much damped by the transverse magnetic field at $N = 0.01$. The x -directional and y -directional transverse fields have the same influences on the wake behind the sphere, which is also confirmed by the identical time history of drag and lift coefficients in figure 8(c).

After vortices are shed from the sphere, they are advected downstream. Figure 9 shows the power spectra of the streamwise velocity at point $(0, 0, 6d)$ behind the sphere for $N = 0$, and for $N = 0.01$ in the x - and y -directions. It is clearly seen that the same shedding frequency $S_t = 0.136$ is found at $N = 0.01$ for x -directional and y -directional transverse magnetic fields, which means that both fields have the same influences on the downstream wake flow. Compared with the case with no magnetic field at $N = 0$, the shedding frequency is unchanged. Hence, the transverse magnetic field affects only the amplitude and not the frequency of vortex shedding. Numerical (Mutschke *et al.* 2001) and experimental (Lahjomri *et al.* 1993) results found that flow past a cylinder with an increasing streamwise magnetic field led to a slightly reduced shedding frequency. Shatrov *et al.* (1997) claimed that an increasing streamwise magnetic field caused a reduction of the mean separation angle of a two-dimensional cylinder flow, which should lead to a slightly smaller shedding frequency. However, for the present sphere case, the separation line during the vortex shedding process is nearly unaffected by the influence of a weak transverse magnetic field at $N = 0.01$. The Lorentz force mainly affects the tilt of the recirculation

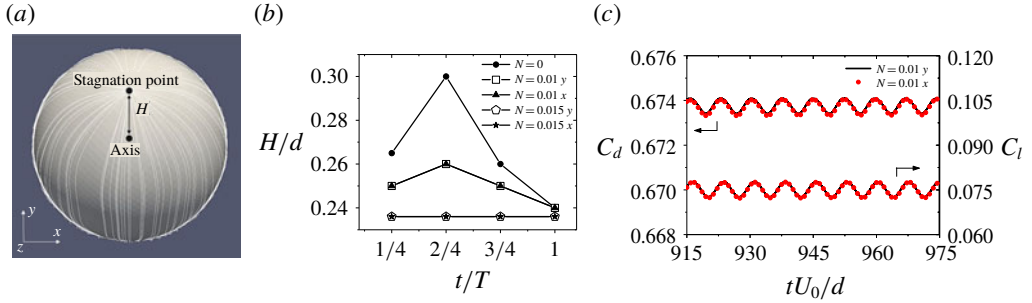


FIGURE 8. Time evolution at $Re = 300$ with different interaction parameters. The magnetic field is along the x - or y -direction. (a) Schematic for the distance length H between the stagnation point and the axis along the sphere centre. (b) Time evolution of distance length during one vortex shedding period T . The time is scaled with T . (c) Time history of drag and lift coefficients. The time is scaled with d/U_0 . These coefficients are both scaled with $\frac{1}{2}\rho U_0^2 A$, where A is the transverse section area of the sphere.

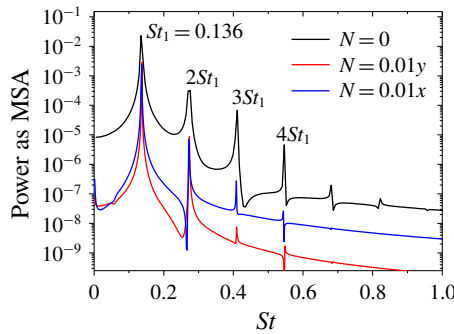


FIGURE 9. Power spectra of the streamwise velocity component at $x=0$, $y=0$, $z=6d$ behind the sphere at $Re = 300$ with $N = 0$ or $N = 0.01$ (semi-log plots). The magnetic field is along the x - or y -direction.

and the separation angle remains unchanged. This may be the reason for the same shedding frequency. Such unchanged shedding frequency phenomenon is also found in the case of flow past a sphere with a streamwise magnetic field (Pan *et al.* 2018). Furthermore, a stronger damping of the superharmonics can be seen in figure 9. The same phenomenon is also reported for a streamwise magnetic field case in Pan *et al.* (2018). For x -directional or y -directional transverse magnetic fields, the different initial angle θ impacts the time scale of the wake going to the final equilibrium state (see § 3.3), which causes the different amplitude of the frequency of the superharmonics in figure 9.

Three-dimensional large-scale vortical structures in the near-wake region of the sphere are shown by streamwise vorticity in figure 10. In figure 8(b), the degree of tilt is greatly damped by the magnetic field, so the smaller tilt converts less azimuthal vorticity into streamwise vorticity. Hence, a smaller streamwise vorticity is shown in figure 10(b).

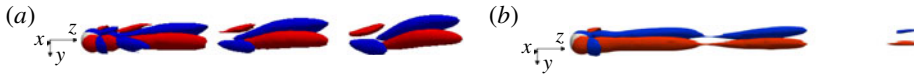


FIGURE 10. Streamwise vortical structures at $Re = 300$ with different interaction parameters: (a) $N = 0$ and (b) $N = 0.01$. Isosurfaces of streamwise vorticity with $\omega_z \pm 0.4$. The red streamwise vorticity is positive while the blue one is negative.

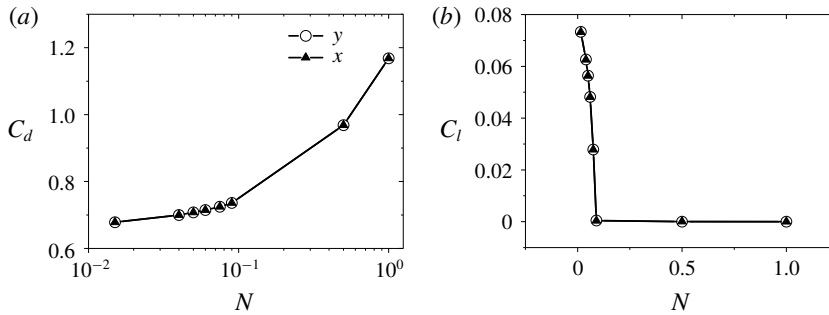


FIGURE 11. Drag and lift coefficients of steady flows at $Re = 300$ versus the interaction parameter with a magnetic field along x - or y -direction: (a) C_d (semi-log plots) and (b) C_l .

3.2.2. Steady flow under an increasing magnetic field

Shatrov *et al.* (1997) reported that the unsteady vortex shedding of a two-dimensional flow past a cylinder would be suppressed and transitioned to a steady flow affected by a transverse magnetic field. Then a stronger transverse magnetic field could lead to a complete suppression of recirculation. Similar results can be found for the present sphere case. Under an increasing magnetic field, the oscillation of the distance length H in figure 8(b) will be completely suppressed. The periodic state transitions to a steady state at $N = 0.015$. But the distance length itself is still larger than zero, which means the tilt of recirculation behind the sphere still exists. The flow is now steady, plane symmetric and a constant lift force is in the symmetry plane. In §3.2.1, x -directional and y -directional transverse magnetic fields have the same influences on unsteady wake structures. This conclusion is also suitable for steady wake structure situations, since figure 11 shows identical drag and lift coefficients. Remember that the flow past a sphere is first simulated for a long enough time and then a transverse magnetic field is imposed. In order to check whether the different initial time instants for imposing a transverse magnetic field have an influence on the final steady state, four time instants of a period as the starting points in figure 8(b) are tested at $N = 0.04$. All results are identical, which indicates that the starting time of imposing a magnetic field does not affect the final results, and the present steady results are consistent. Furthermore, the lift coefficient in figure 11(b) decreases with an increasing magnetic field and then remains zero. It should be noted that the non-zero lift zone corresponds to a plane symmetric state with tilt of recirculation behind the sphere while the flow in the zero lift zone corresponds to a double plane symmetric state. Here, a transition occurs at $C_l = 0$.

Figure 12 shows detailed changes of topological structures, indicating that the wake structure is symmetric in the P-symmetry plane and the small left spiral in the N-symmetry plane will grow until it becomes the same as the right spiral. Now the lift force is zero and a transition from a steady plane symmetric flow to a

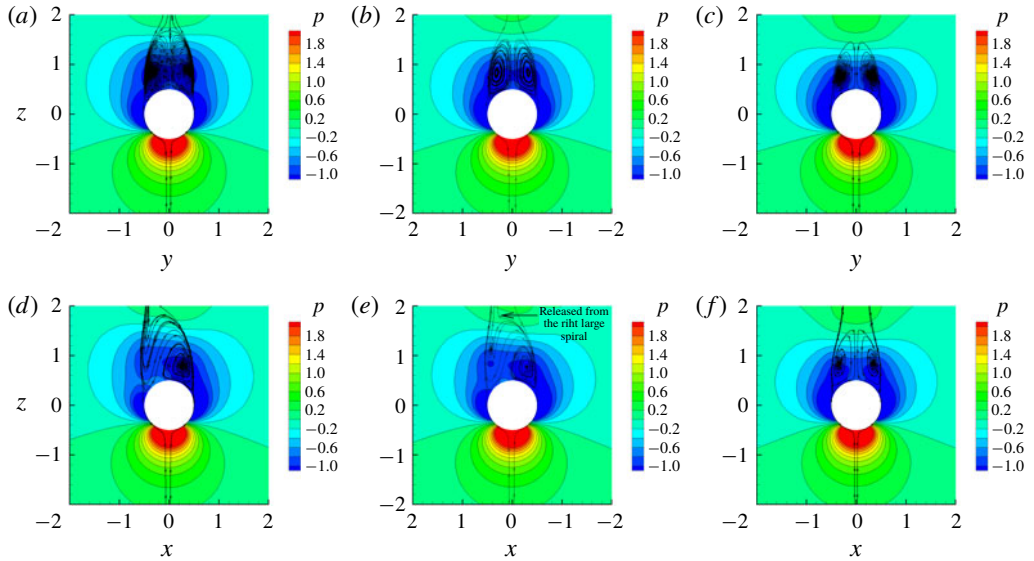


FIGURE 12. Pressure contours and streamlines in the symmetry plane at $Re = 300$ steady flow with different interaction parameters. The magnetic field direction is along the y -direction. (a) P-symmetry plane at $N = 0.015$. (b) P-symmetry plane at $N = 0.04$. (c) P-symmetry plane at $N = 0.09$. (d) N-symmetry plane at $N = 0.015$. (e) N-symmetry plane at $N = 0.04$. (f) N-symmetry plane at $N = 0.09$.

steady double plane symmetric one occurs. With a further increasing magnetic field, the topological structure behind the sphere at $Re = 300$ will go through the same patterns that happened at $Re = 150$ in figure 3. With Reynolds numbers up to 300, a steady axisymmetric flow and an unsteady flow affected by a transverse magnetic field have been investigated. It is noted that, for a steady plane symmetric flow at $210 < Re < 270$, the topological structure of the wake behind the sphere affected by a transverse magnetic field will go through the same changes as the steady flow at $Re = 300$ shown in figure 12. They both experience the small left spiral growing, a transition from plane symmetry to double plane symmetry. Hence, the results are not repeatedly presented here.

The wake structure behind the sphere will change from an unsteady plane symmetric pattern to a steady plane symmetric one when affected by a transverse magnetic field. At this stage, the recirculation at the rear of the sphere still exists. Its wake structure has a similar topological structure with the case at $210 < Re < 270$ in the absence of a magnetic field. An effective viscosity concept in a previous investigation (Pan *et al.* 2018) can be used to understand this phenomenon with a magnetic damping effect. This theory claims that the Lorentz force action on the flow can be seen as an effective viscosity and that increasing the magnetic field is equivalent to adding effective viscosity into a corresponding hydrodynamic flow case, which is equivalent to decreasing the effective Reynolds number. Consequently, the change of wake structure affected by an increasing magnetic field will experience a similar change of wake structure in a hydrodynamic flow case with decreasing Reynolds number. Hence, a so-called ‘reversion phenomenon’ (Pan *et al.* 2018) is also found, which indicates that the topological structure behind the sphere at a higher Reynolds number with a certain interaction parameter corresponds to a

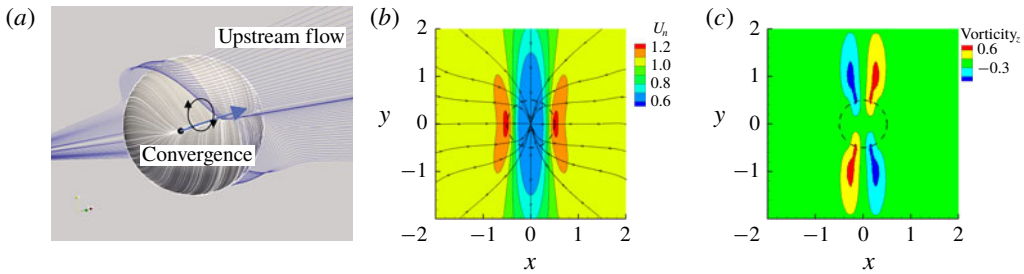


FIGURE 13. Detailed wake flow at $Re = 300$ with $N = 16$. (a) Three-dimensional streamlines at the rear of the sphere. The blue arrow is a jet flow, which is caused by convergence of upstream flow. (b) Contour of the streamwise velocity norm U_n at the slice $z = 1d$ behind the sphere. The velocity U_n is scaled with the inlet velocity. Traces of cross-flow velocity are projected on the slice. (c) Streamwise vorticity contour at the slice $z = 1d$ behind the sphere. The profile of the sphere is indicated by a dashed circle.

lower-Reynolds-number case with a lower interaction parameter. Finally, all wake structures will be damped to be a double plane symmetric state with a strong transverse magnetic field.

The double plane symmetric wake is further discussed below. Figure 13 shows a detailed wake flow at $Re = 300$ with $N = 16$. With the reversion phenomenon, the topological structure in figure 13(a) is double plane symmetric, which corresponds to the same topological structure at $Re = 150$ with $N = 4$ in figure 3(d). Upstream flows converge at two sides of the straight separation line by the action of the Lorentz force. Under the mass conservation constraint, the flow velocity at these two zones is faster than the surrounding flow, as shown in figure 13(a,b), so there will be a jet flow, which heads downstream and meets with the low-speed outer upstream flow. Then the upstream flow is pushed away and has a swirl velocity to move downstream. Such interaction converts to a streamwise vorticity. Figure 13(c) plots the streamwise vorticity contours at the slice $z = 1d$ behind the sphere, which confirms again that the wake structure is double plane symmetric.

3.3. Preferred orientation of the vortex symmetry plane

In § 3.2, it was reported that the wake structure behind the sphere showed the same quantitative changes affected by transverse magnetic fields with identical intensity and different angle θ , such as the tilt of recirculation, vortex shedding frequency, drag coefficient and lift coefficient. Now we pay attention to the relationship between the orientation of the symmetry plane and the transverse magnetic field. The dash-dotted line in figure 14 represents the symmetry plane at $Re = 300$ with $N = 0$. As can be seen, after being affected by the x -directional or y -directional transverse magnetic field at $N = 0.01$, the new symmetry plane denoted by the solid line at time instant $T = 300$ will rotate and tend to be perpendicular to the magnetic field. Apart from the unsteady flow, we also examine the steady plane symmetric flow in § 3.2.2. Detailed topological structures of these flows are shown in figure 12. Such ring vortex shifting generates a lift force within the symmetry plane, so the lift force orientation can represent the orientation of the symmetry plane. The lift force in the transverse plane can be decomposed into x - and y -components. Detailed lift force coefficients affected by two transverse magnetic fields are plotted in figure 15(a). The direction from the

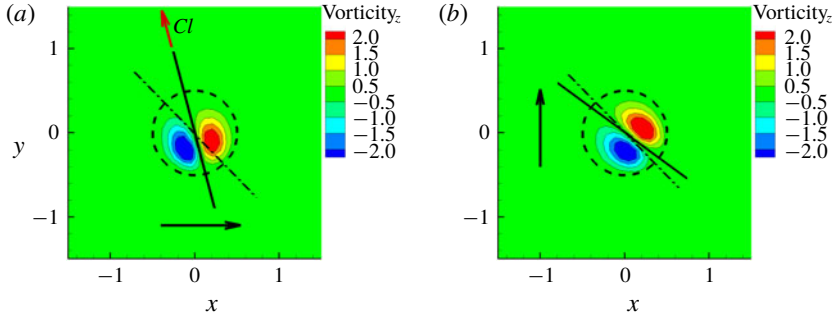


FIGURE 14. Cross-section of streamwise vortical structures at 1.5 diameters behind the sphere is plotted at $Re = 300$ with $N = 0.01$ at time instant $T = 300$ (not final stable state): (a) x -directional magnetic field and (b) y -directional magnetic field. The dash-dotted line and solid line represent the orientation of the original and new symmetry planes, respectively. The black and red arrows mean the magnetic field direction and the lift force direction, respectively. The profile of the sphere is indicated by a dashed circle.

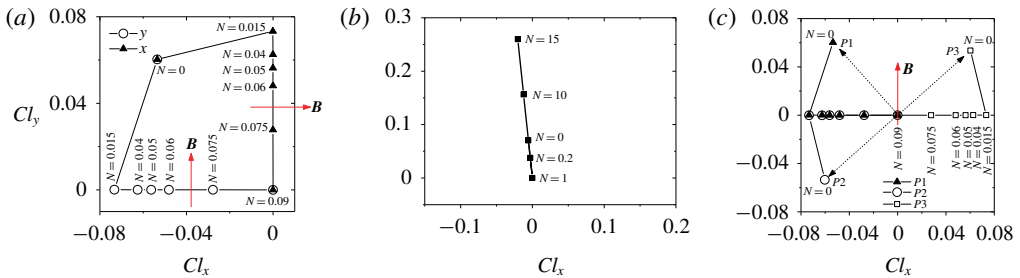


FIGURE 15. The orientation of the wake structure tends to be perpendicular to a transverse magnetic field. The red arrow represents the magnetic field direction. (a) Lift force Cl_x-Cl_y plot at $Re = 300$ with different interaction parameters under the influence of a transverse magnetic field. (b) Lift force Cl_x-Cl_y plot at $Re = 250$ with different interaction parameters under the influence of a streamwise magnetic field (Pan *et al.* 2018). (c) Lift force Cl_x-Cl_y plot at $Re = 300$ with different initial symmetry planes under the influence of a transverse magnetic field. The dashed arrow represents the initial orientation of the symmetry plane at $N = 0$.

coordinate origin to the data point of the lift force represents the orientation of the symmetry plane. It is clearly seen that, under the influence of a transverse magnetic field, this orientation is completely perpendicular to the magnetic field in the final equilibrium state.

Figure 16 plots a schematic of how the Lorentz force affects the orientation of the symmetry plane. The tilt of recirculation behind the sphere is simply represented by a small and large spiral. The orientation is along these two spirals. In fact, the physical mechanism here is similar to the case in § 3.1. The moving trend of upstream flow affected by the action of the Lorentz force in figure 16(a) will rotate the orientation, and the faster upstream flow in zone D in figure 16(b) will squeeze the orientation. These two effects finally make the orientation lie in the N -symmetry plane, which is perpendicular to the magnetic field. Further details of the tilt of recirculation behind the sphere are plotted in figure 12(e). Some streamlines from the large spiral directly

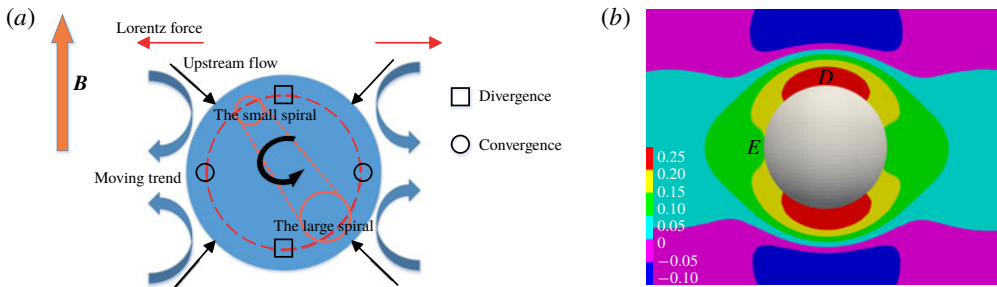


FIGURE 16. Lorentz force at $Re = 300$, $N = 0.04$ in a front view. The flow direction is from inside to outside. (a) Schematic for the moving trend of the upstream flow, which will affect the orientation of the symmetry plane. (b) The z -component of the Lorentz force contours in a section $0.35d$ away from the sphere centre.

flow downstream. However, this is not the case for the similar topological structure affected by a streamwise magnetic field in Pan *et al.* (2018). Since the moving trend of upstream flow not only rotates the orientation of the symmetry plane, but also converges flow near the N-symmetry plane, this will squeeze flow in the large spiral and make some flows spiral outwards and head downstream. The orientation of the symmetry plane at $Re = 250$ affected by a streamwise magnetic field in Pan *et al.* (2018) is also examined. However, the original symmetry plane at $N = 0$ is unchanged in figure 15(b), which is different from the present transverse magnetic field case.

For the orientation of the symmetry plane without a magnetic field, the orientation in principle is random but is actually determined by perturbations in experiments or numerical biases (Johnson & Patel 1999). It has been reported in Ghidersa & Dušek (2000) that the symmetry plane can be selected randomly by perturbation with a spectral/spectral-element discretization method. However, in the present finite-volume-type numerical method it is difficult to impose a perturbation for a certain direction in a flow around a fixed sphere. In order to obtain different initial angle θ , one easy way is to change the transverse magnetic field direction. As seen in figure 15(a), the orientation of the symmetry plane is located at $N = 0$. Three kinds of magnetic field directions are considered, which are along the y -axis positive direction, the x -axis positive direction and the x -axis negative direction. These three magnetic fields have different initial angle θ with the symmetry plane. Since the flow configuration and the numerical model are axisymmetric, the whole system of these three magnetic fields can be rotated around the z -axis to be parallel to the y -direction, as shown in figure 15(c). Now three cases with different initial symmetry planes at $N = 0$ are affected by a transverse magnetic field. The lift force $Cl_x - Cl_y$ plot as in figure 15(a) is given in figure 15(c). Owing to the symmetry breaking that occurs when going from the solution with two symmetry planes at $N = 0.09$ to the solution with only one symmetry plane with $N < 0.09$, two equivalent solutions with one symmetry plane exist. Hence, the transition occurs at a pitchfork bifurcation.

Ern *et al.* (2012) reported that the wake structure behind a free-moving particle was related to its trajectories. So it is possible that the transverse magnetic field can control the trajectory of a free-moving particle by changing the orientation of its wake structure. A case is given below to show this control feature.

The freely rising sphere case at $G = 165$, $m^* = 0.5$ in the absence of a magnetic field is chosen. Here, $G = U_0 d / \nu$ is the Galileo number, which replaces the

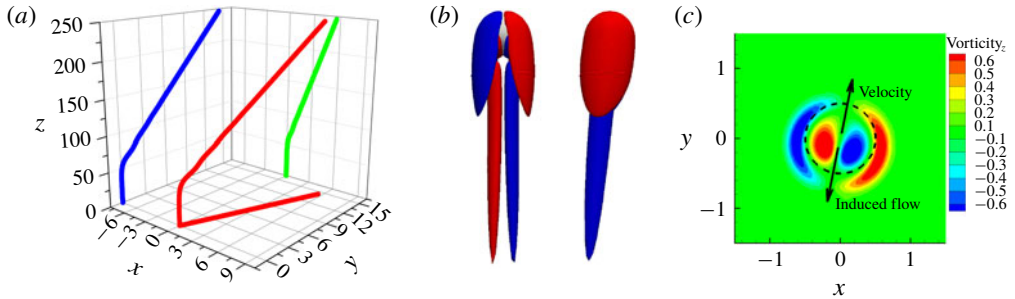


FIGURE 17. Freely rising sphere at $G = 165$, $m^* = 0.5$ without a magnetic field. (a) Oblique trajectory. (b) Isosurfaces of streamwise vorticity with $\omega_z \pm 0.3$. The red streamwise vorticity is positive while the blue one is negative. (c) Cross-section plot of streamwise vortical structures at one diameter behind the sphere. The profile of the sphere is indicated by a dashed circle.

Reynolds number in a moving-body problem; $U_0 = \sqrt{|1 - m^*|gd}$ is the gravitational velocity scale, where g is the acceleration of gravity and m^* measures the ratio of particle density to fluid density. A moving-frame method coupled with sphere motion equations (Pan, Zhang & Ni 2019) is used to simulate a freely rising sphere. Figure 17(a) shows an oblique trajectory of the sphere, which agrees with the numerical result (Jenny, Dušek & Bouchet 2004) and the experimental result (Horowitz & Williamson 2010). Figure 17(b) shows a double-threaded wake consisting of streamwise counter-rotating vortices. It is clearly seen that the wake structure is plane symmetric. Furthermore, these two vortices will induce a flow with the right-hand rule and then a force will be exerted on the sphere under the law of interaction, which leads to a horizontal velocity to compensate this force, as shown in figure 17(c). It is noted that the horizontal velocity is along the symmetry plane. Hence, the horizontal velocity can represent the orientation of the wake structure.

The reason to choose such a freely rising sphere is that it has a similar wake structure to a flow past a fixed sphere in § 3.2.2. They are both plane symmetric with a double-threaded wake. After the freely rising sphere reaches its stable state, x -directional and y -directional transverse magnetic fields are imposed respectively to show its control feature to the trajectory of the freely rising sphere. The horizontal velocity of the freely rising sphere is used to represent the direction of motion of the sphere in the horizontal plane. As shown in figure 18, under the influence of a transverse magnetic field, the horizontal velocity tends to be perpendicular to the magnetic field. The reason is that the transverse magnetic field rotates the wake structure behind the freely rising sphere to be perpendicular to itself, as shown in figure 19. Assuming one is standing on the free sphere centre to observe the flow field, the physical mechanism of wake structure rotation is similar to the fixed-sphere case. The only difference is that there is no constraint on the degrees of freedom of a freely rising sphere. Hence, the rotation of the wake structure will rotate the freely rising sphere by viscosity force, which will facilitate the fluid–solid system moving into a new equilibrium state. As shown in figure 17(c), the smaller the streamwise vorticity, the weaker induced flow it has, leading to a smaller horizontal velocity. Figure 19 shows that the streamwise vorticity becomes smaller under the damping effect of an increasing magnetic field. Its variation trend is the same as the change of the horizontal velocity in figure 18.

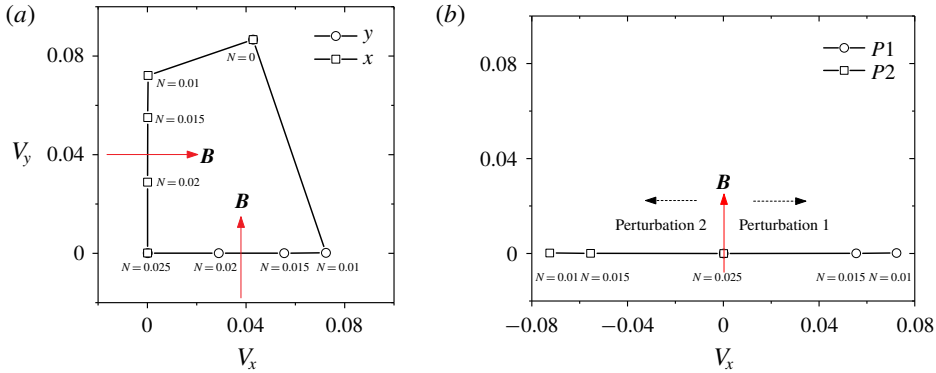


FIGURE 18. Magnetic field can control a freely rising sphere moving at $G = 165$, $m^* = 0.5$ under the influence of a transverse magnetic field. (a) Transverse velocity V_x – V_y plot for x - and y -directional magnetic field. (b) Transverse velocity V_x – V_y plot with two opposite small perturbations. The free-moving sphere is first stable at $N = 0.025$ and then the magnetic field changes to $N = 0.01$ and $N = 0.015$ with a small x -direction perturbation of horizontal velocity exerted on the sphere.

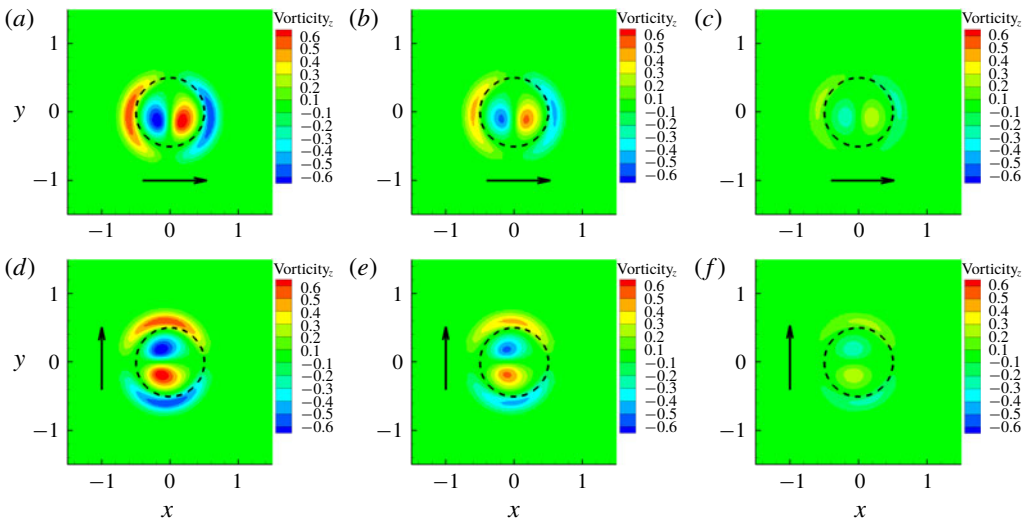


FIGURE 19. Cross-section plots of streamwise vortical structures affected by a transverse magnetic field at one diameter behind the freely rising sphere at $G = 165$, $m^* = 0.5$: (a) $N = 0.01$, (b) $N = 0.015$, (c) $N = 0.02$, (d) $N = 0.01$, (e) $N = 0.015$ and (f) $N = 0.02$. The arrow indicates the magnetic field direction. The profile of the sphere is indicated by a dashed circle.

As shown in figure 18(a), a horizontal velocity transition occurs at $N = 0.025$, where the motion of the free-moving sphere transitions from an oblique trajectory to a vertical one. A small velocity perturbation along the x -axis positive direction or the x -axis negative direction is exerted on the free sphere when it rises vertically and, at the same time, the transverse magnetic field decreases from $N = 0.025$ to $N = 0.015$ or $N = 0.01$. Figure 18(b) shows two equivalent solutions where one symmetry plane exists. The transition also occurs at a pitchfork bifurcation.

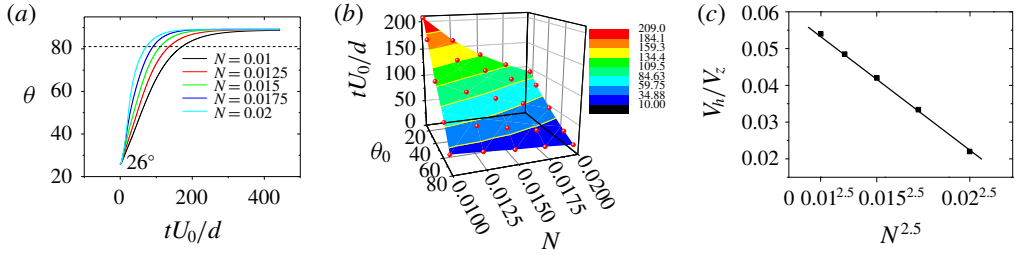


FIGURE 20. Control features at $G = 165$, $m^* = 0.5$ with different initial angles and interaction parameters. The time is scaled with d/U_0 , where U_0 is the gravitational velocity. (a) Time history of the angle θ . The dashed line represents a threshold angle $\theta_t = 81^\circ$, which means the transverse velocity is 90% perpendicular to the magnetic field. (b) The evolving time for different initial angles reaching 90% perpendicular to a magnetic field. Solid points represent results of different cases. (c) Horizontal migration ratio defined by V_h/V_z , where V_h and V_z are terminal horizontal and vertical velocities.

Some control features are discussed here. Figure 20(a) plots a time history of the angle θ with an initial angle $\theta_0 = 26^\circ$. The most attractive feature is that the transverse magnetic field can control the horizontal motion of the free sphere to be perpendicular to itself. Here, a threshold angle $\theta_t = 81^\circ$ is defined, which means the angle θ reaches 90% perpendicular to a magnetic field and one can say that the control effect is obvious when $\theta > \theta_t$. In order to give a systematic investigation of the influence of the initial angle θ_0 and the magnetic field intensity N on the temporal evolution of the angle θ , a total of 25 cases are simulated. Figure 20(b) shows the evolving time of the angle θ from the initial angle θ_0 to the threshold angle θ_t . It is clearly seen that it takes less time for a strong magnetic field to reach the angle θ_t . Apart from the evolving time, a horizontal migration ratio is defined by V_h/V_z , where V_h and V_z are the terminal horizontal and vertical velocities of the free sphere. The horizontal migration ratio decreases with increasing magnetic field and shows a linear dependence of $N^{2.5}$ in the range $0.01 \leq N \leq 0.02$ in figure 20(c).

Further consideration about the temporal evolution of the angle θ to reach the equilibrium state is given in figure 21. In § 3.2.2, an effective viscosity concept is used to explain the ‘reversion phenomenon’, which claims that a magnetic damping effect is equivalent to adding effective viscosity into the case and this case reverts to a lower-Reynolds-number case with a lower interaction parameter. The ‘reversion phenomenon’ inspires us to use the magnetic damping time $\tau = (\sigma B^2/\rho)^{-1}$ to scale the evolving time in figure 20(b). The interaction parameter $N = \sigma B^2 d/\rho U_0$ can be reformed as $N = d/U_0 \tau$, so that we have the relation $\tau = d/U_0 N$. For the present investigations, d/U_0 is a fixed value; hence with the time scaling τ , the three-dimensional plot in figure 20(b) is reduced to a two-dimensional plot in figure 21(a), where the magnetic damping effects shrink together. This can be more clearly seen by comparing figure 20(a) and figure 21(a). The shape of the angle θ evolving curve is like a hyperbolic tangent function $\theta = 90 \tanh(\beta T)$, where β is a parameter. As can be seen in figure 21(a), the time history of the angle θ can collapse together by horizontal translation and the collapsed curve is characterized by a hyperbolic tangent function. So for a case with an initial angle θ_0 , the temporal evolution of the angle θ can be easily fitted with a hyperbolic tangent function

$$\theta' = \tanh(\beta T + \text{atanh}(\theta'_0)). \tag{3.1}$$

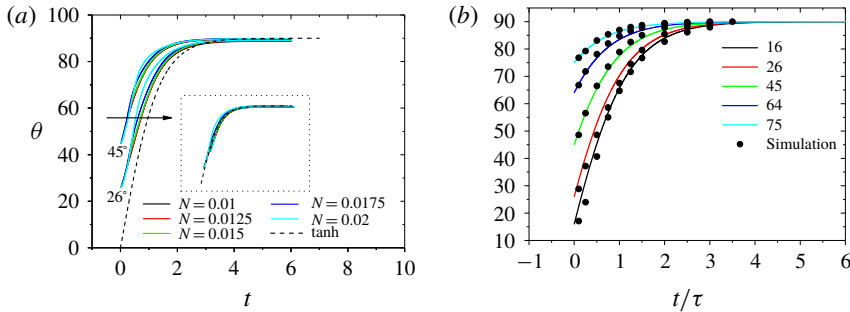


FIGURE 21. Evolution of the transient time to reach the equilibrium angle at $G = 165$, $m^* = 0.5$ with different initial angles and interaction parameters. The time is scaled with the magnetic damping time $\tau = (\sigma B^2/\rho)^{-1}$. (a) Time history of the angle θ . The dashed curve represents a hyperbolic tangent function. Solid curves can collapse to the dashed curve by horizontal translation, as the black arrow shows. (b) The comparison between fitted curves and simulation results at $N = 0.015$.

Here, $\theta' = \theta/90$ and $\theta'_0 = \theta_0/90$. It is noted that here the evolution time is scaled with the magnetic damping time, $T = t/\tau = tNU_0/d$. With some mathematical operations, the inverse function of the above equation is given as

$$T = \frac{1}{\beta} \operatorname{atanh} \left(\frac{\theta' - \theta'_0}{1 - \theta'\theta'_0} \right). \tag{3.2}$$

The only unknown parameter β can be easily obtained by linear fitting with the 25 simulation results, which gives $\beta = 0.75$. Figure 21(c) shows good agreement between the fitted curves plotted with (3.1) and the simulation results.

The control feature of the transverse magnetic field is attractive. The present work is the first time that the field–wake–trajectory control mechanism has been analysed for a particle freely moving in MHD flows.

3.4. Drag and lift coefficients

Pan *et al.* (2018) reported that the drag coefficient was proportional to $N^{1/2}$ for a strong streamwise magnetic field. A similar result is also found here for a strong transverse magnetic field. Figures 22(a) and 22(b) show two linear relationships. The drag coefficient is proportional to $N^{2/3}$ for small interaction parameters or $N^{1/2}$ for large interaction parameters. The threshold between these two drag coefficient regimes is approximately $N = 4$. Delacroix & Davoust (2018) found that the drag coefficient in the presence of a weak transverse magnetic field is proportional to $N^{0.65}$. However, for large interaction parameters, drag measurements in Kalis *et al.* (1966) are proportional to $N^{1/2}$. Here, a qualitative analysis is used to explain the drag law $C_d \propto N^{1/2}$ for large interaction parameters. The existence of a sphere can be seen as a finite disturbance in the inflow, which results in two main physical phenomena. Part of the finite disturbance near the sphere that is perpendicular to the magnetic field is a thin Hartmann boundary layer. Müller & Bühler (2013) reported that the dominant role of the Hartmann boundary layer was responsible for electromagnetic pressure losses originating from the Joule dissipation effect. They found that the pressure drop was proportional to $N^{1/2}$. Hence, the energy loss in the Hartmann

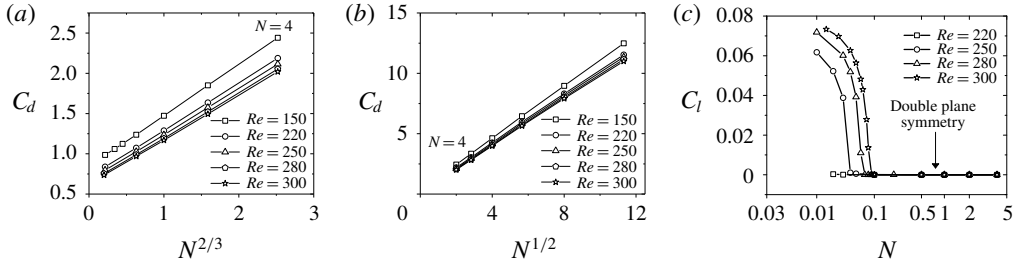


FIGURE 22. Drag and lift coefficients versus the interaction parameter. (a) Linear dependence of drag coefficient versus $N^{2/3}$ for small interaction parameters. (b) Linear dependence of drag coefficient versus $N^{1/2}$ for large interaction parameters. (c) Lift coefficient in steady flows with different Reynolds numbers versus the interaction parameter.

<i>Re</i>	220	250	280	300
<i>N</i>	0.01	0.04	0.065	0.085

TABLE 2. The transition points of lift coefficient $C_l=0$ at steady flows for different Reynolds numbers affected by a transverse magnetic field.

boundary layer by the Joule dissipation effect is proportional to $N^{1/2}$. The other part of the finite disturbance is flow around the sphere and this lateral movement flow sweeps a portion of the magnetic field sideways. Hence, an Alfvén wave is created, which can propagate the finite disturbance and energy away along the magnetic field (Davidson 2001; Moreau 2013). It is noted that such a process is similar to the streamwise magnetic field case (Pan *et al.* 2018), for which the energy propagated by an Alfvén wave is also proportional to $N^{1/2}$. The drag law may be interpreted from the perspective of the energy. Assume that we set the coordinate system fixed on the sphere centre and make the sphere move with the inlet flow velocity. Now, the power created from the drag force pushing the sphere mainly contributes to the energy carried away by the Alfvén wave and the pressure drop power (Joule dissipation) in the Hartmann boundary layer. So for a large interaction parameter, there is a drag law $C_d \propto N^{1/2}$.

In § 3.2, for a weak magnetic field at $N=0.01$, the unsteady vortex shedding flow at $Re=300$ will be damped. The amplitude of tilt of recirculation behind the sphere becomes smaller. With an increasing magnetic field at $N=0.015$, the unsteady flow transitions to a steady flow with a constant lift force within the symmetry plane. Figure 22(c) plots the steady part of the lift coefficient with different Reynolds numbers versus the interaction parameter. The lift force decreases with increasing magnetic field and then remains zero. The non-zero lift force zone corresponds to a plane symmetric state with a tilt of recirculation behind the sphere and the flow in the zero lift zone corresponds to a double plane symmetric state. The inflection points of lift coefficients at $C_l=0$ represent a transition. Detailed transition values are given in table 2. It is noted that the transition occurs at a pitchfork bifurcation. In order to define various wake structures and transition processes, a total of 112 cases are performed. Figure 23 gives the map of regimes for wake patterns behind a sphere in the $\{N, Re\}$ plane.

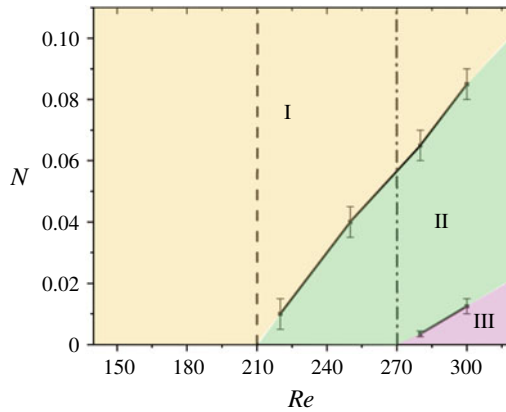


FIGURE 23. Map of regimes for wake patterns behind a sphere in the $\{N, Re\}$ plane. The dashed and dash-dotted lines correspond to the hydrodynamics first and second bifurcation, respectively. Regime I is a steady double plane symmetric state. Regime II is a steady plane symmetric state. The last regime III is an unsteady plane symmetric state.

4. Conclusions

The wake structure of a flow past a sphere with Reynolds numbers up to 300 under the influence of an imposed transverse magnetic field has been simulated and analysed in detail. For a steady axisymmetric flow affected by a transverse magnetic field, the upstream flow diverges from the symmetry plane parallel to the magnetic field and converges to the symmetry plane normal to it. The wake flow is double plane symmetric. For an unsteady vortex shedding flow, only the amplitude of vortex shedding is damped but the frequency remains unchanged. Under an increasing magnetic field with the interaction parameter $N = 0.015$, vortex shedding is totally suppressed and the wake structure transitions to a steady plane symmetric pattern, for which a tilt of recirculation behind the sphere exists. Such ring vortex shifting produces a constant lift force. With a further increasing magnetic field, the lift force decreases and reaches zero. Now, the wake structure transitions to a double plane symmetric state, where the transition occurs at a pitchfork bifurcation. A total of 112 cases among three kinds of wake structure patterns are summarized in the $\{N, Re\}$ plane.

Wake structures at Reynolds numbers from 210 to 300 without a magnetic field are plane symmetric. There will be an angle θ between the orientation of the symmetry plane and the transverse magnetic field. Transverse magnetic fields with identical intensity and different initial angle θ have the same influence on the wake structure. However, the orientation of the symmetry plane tends to be perpendicular to the transverse magnetic field. Furthermore, we show the field–wake–trajectory control mechanism for a sphere freely moving in MHD flows and consider the temporal evolution of the angle θ related to the initial angle θ_0 and the magnetic field intensity N . The control feature of a transverse magnetic field will be investigated more in the future.

A so-called ‘reversion phenomenon’ is also found. It describes that the topological structure behind the sphere with a higher Reynolds number and a certain interaction parameter corresponds to a lower-Reynolds-number case with a lower interaction parameter. An effective viscosity concept can explain this phenomenon. Finally, all

wake structures will be in a double plane symmetric state with a strong transverse magnetic field. Furthermore, two linear relationships of the drag coefficient are found. One is proportional to $N^{2/3}$ for small interaction parameters; the other is proportional to $N^{1/2}$ for large interaction parameters; and the threshold value between these two regimes is approximately $N = 4$.

Acknowledgements

The authors gratefully acknowledge the support from NSFC (no. 51636009 and no. 51776194) and from CAS (no. XDB22040201). The authors also appreciate the comments of the anonymous reviewers, which significantly improved the manuscript.

REFERENCES

- BRANOVER, H., EIDELMAN, A. & NAGORNY, M. 1995 Use of turbulence modification for heat transfer enhancement in liquid metal blankets. *Fusion Engng Des.* **27**, 719–724.
- CHESTER, W. 1957 The effect of a magnetic field on Stokes flow in a conducting fluid. *J. Fluid Mech.* **3** (3), 304–308.
- DAVIDSON, P. A. 2001 *An Introduction to Magnetohydrodynamics*. Cambridge University Press.
- DELACROIX, J. & DAVOUST, L. 2018 Drag upon a sphere suspended in a low magnetic-Reynolds number MHD channel flow. *Phys. Rev. Fluids* **3**, 123701.
- EL-KADDAH, N., PATEL, A. D. & NATARAJAN, T. T. 1995 The electromagnetic filtration of molten aluminum using an induced-current separator. *JOM J. Miner. Met. Mater. Soc.* **47** (5), 46–49.
- ERN, P., RISSO, F., FABRE, D. & MAGNAUDET, J. 2012 Wake-induced oscillatory paths of bodies freely rising or falling in fluids. *Annu. Rev. Fluid Mech.* **44**, 97–121.
- FABRE, D., AUGUSTE, F. & MAGNAUDET, J. 2008 Bifurcations and symmetry breaking in the wake of axisymmetric bodies. *Phys. Fluids* **20** (5), 051702.
- FRANK, M., BARLEON, L. & MÜLLER, U. 2001 Visual analysis of two-dimensional magnetohydrodynamics. *Phys. Fluids* **13** (8), 2287–2295.
- GHIDERSA, BRĂDUȚ & DUŠEK, J. 2000 Breaking of axisymmetry and onset of unsteadiness in the wake of a sphere. *J. Fluid Mech.* **423**, 33–69.
- GOLDSWORTHY, F. A. 1961 Magnetohydrodynamic flows of a perfectly conducting, viscous fluid. *J. Fluid Mech.* **11** (4), 519–528.
- HOROWITZ, M. & WILLIAMSON, C. H. K. 2010 The effect of Reynolds number on the dynamics and wakes of freely rising and falling spheres. *J. Fluid Mech.* **651**, 251–294.
- JENNY, M., DUŠEK, J. & BOUCHET, G. 2004 Instabilities and transition of a sphere falling or ascending freely in a Newtonian fluid. *J. Fluid Mech.* **508**, 201–239.
- JOHNSON, T. A. & PATEL, V. C. 1999 Flow past a sphere up to a Reynolds number of 300. *J. Fluid Mech.* **378**, 19–70.
- KALIS, K., SLYUSAREV, N., TSINOBER, A. & SHTERN, A. 1966 Resistance of bluff bodies at high Stewart numbers. *Magnetohydrodynamics* **2** (4), 152–153.
- KANARIS, N., ALBETS, X., GRIGORIADIS, D. & KASSINOS, S. 2013 Three-dimensional numerical simulations of magnetohydrodynamic flow around a confined circular cylinder under low, moderate, and strong magnetic fields. *Phys. Fluids* **25** (7), 074102.
- LAHJOMRI, J., CAPÉLAN, P. & ALEMANY, A. 1993 The cylinder wake in a magnetic field aligned with the velocity. *J. Fluid Mech.* **253**, 421–448.
- LIGHTHILL, M. J. 1963 Boundary layer theory. In *Laminar Boundary Layers* (ed. L. Rosenhead), pp. 46–103. Oxford University Press.
- MAXWORTHY, T. 1962 Measurements of drag and wake structure in magneto-fluid dynamic flow about a sphere. In *Heat Transfer and Fluid Mechanics Institute Annual Meeting*, pp. 197–205. Stanford University Press.
- MITTAL, R. 1999 Planar symmetry in the unsteady wake of a sphere. *AIAA J.* **37** (3), 388–390.
- MOREAU, R. J. 2013 *Magnetohydrodynamics*. Springer.

- MÜCK, B., GÜNTHER, C., MÜLLER, U. & BÜHLER, L. 2000 Three-dimensional MHD flows in rectangular ducts with internal obstacles. *J. Fluid Mech.* **418**, 265–295.
- MÜLLER, U. & BÜHLER, L. 2013 *Magnetofluidynamics in Channels and Containers*. Springer.
- MUTSCHKE, G., GERBETH, G., SHATROV, V. & TOMBOULIDES, A. 2001 The scenario of three-dimensional instabilities of the cylinder wake in an external magnetic field: a linear stability analysis. *Phys. Fluids* **13** (3), 723–734.
- NATARAJAN, R. & ACRIVOS, A. 1993 The instability of the steady flow past spheres and disks. *J. Fluid Mech.* **254**, 323–344.
- NI, M.-J., MUNIPALLI, R., HUANG, P., MORLEY, N. B. & ABDOU, M. A. 2007 A current density conservative scheme for incompressible MHD flows at a low magnetic Reynolds number. Part II: On an arbitrary collocated mesh. *J. Comput. Phys.* **227** (1), 205–228.
- ORMIÈRES, D. & PROVANSAL, M. 1999 Transition to turbulence in the wake of a sphere. *Phys. Rev. Lett.* **83** (1), 80–83.
- PAN, J.-H., ZHANG, N.-M. & NI, M.-J. 2018 The wake structure and transition process of a flow past a sphere affected by a streamwise magnetic field. *J. Fluid Mech.* **842**, 248–272.
- PAN, J.-H., ZHANG, N.-M. & NI, M.-J. 2019 Instability and transition of a vertical ascension or fall of a free sphere affected by a vertical magnetic field. *J. Fluid Mech.* **859**, 33–48.
- PIER, B. 2008 Local and global instabilities in the wake of a sphere. *J. Fluid Mech.* **603**, 39–61.
- SARRIS, I. E., ZIKOS, G. K., GRECOS, A. P. & VLACHOS, N. S. 2006 On the limits of validity of the low magnetic Reynolds number approximation in MHD natural-convection heat transfer. *Numer. Heat Transfer* **50** (2), 157–180.
- SEKHAR, T. V. S., SIVAKUMAR, R. & KUMAR, T. R. 2005 Magnetohydrodynamic flow around a sphere. *Fluid Dyn. Res.* **37** (5), 357–373.
- SHATROV, V., MUTSCHKE, G. & GERBETH, G. 1997 Numerical simulation of the two-dimensional flow around a circular cylinder. *Magnetohydrodynamics* **33** (1), 2–10.
- TOMBOULIDES, A. G. & ORSZAG, S. A. 2000 Numerical investigation of transitional and weak turbulent flow past a sphere. *J. Fluid Mech.* **416**, 45–73.
- YONAS, G. 1967 Measurements of drag in a conducting fluid with an aligned field and large interaction parameter. *J. Fluid Mech.* **30** (4), 813–821.
- ZHENG, T. X., ZHONG, Y. B., LEI, Z. S., REN, W. L., REN, Z. M., DEBRAY, F., BEAUGNON, E. & FAUTRELLE, Y. 2015 Effects of high static magnetic field on distribution of solid particles in BiZn immiscible alloys with metastable miscibility gap. *J. Alloys Comps* **623**, 36–41.